TECHNISCHE UNIVERSITÄT WIEN

AUTOMATION & CONTROL INSTITUTE
INSTITUT FÜR AUTOMATISIERUNGS- & REGELUNGSTECHNIK

This document contains a post-print version of the paper

Two Illustrative Examples to Show the Potential of Thermography for Process Monitoring and Control in Hot Rolling

authored by **F. Schausberger, K. Speicher, A. Steinboeck, M. Jochum, and A. Kugi**

and published in *Proceedings of the 4th IFAC Workshop on Mining, Mineral and Metal Processing (MMM).*

The content of this post-print version is identical to the published paper but without the publisher's final layout or copy editing. Please, scroll down for the article.

Cite this article as:

F. Schausberger, K. Speicher, A. Steinboeck, M. Jochum, and A. Kugi, "Two illustrative examples to show the potential of thermography for process monitoring and control in hot rolling", in *Proceedings of the 4th IFAC Workshop on Mining, Mineral and Metal Processing (MMM)*, vol. 48, Oulu, Finland, 2015, pp. 48–53. DOI: 10.1016/j.ifacol.2015.10.076

BibTex entry:

```
@Inproceedings{Schausberger15,
  Title = {Two Illustrative Examples to Show the Potential of Thermography for Process Monitoring and
      Control in Hot Rolling},
  Author = {Schausberger, F. and Speicher, K. and Steinboeck, A. and Jochum, M. and Kugi, A.},
  Booktitle = {Proceedings of the 4th IFAC Workshop on Mining, Mineral and Metal Processing (MMM)},
  Year = {2015},

  Address = {Oulu, Finland},
  Month = {25.08. - 28.08.},
  Number = {17},
  Pages = {48--53},
  Volume = {48},

  Doi = {10.1016/j.ifacol.2015.10.076},
  ISSN = {2405-8963}
}
```

Link to original paper:

http://dx.doi.org/10.1016/j.ifacol.2015.10.076

Read more ACIN papers or get this document:

http://www.acin.tuwien.ac.at/literature

Contact:

Automation and Control Institute (ACIN)
TU Wien
Gusshausstrasse 27-29/E376
1040 Vienna, Austria

Internet: www.acin.tuwien.ac.at
E-mail: office@acin.tuwien.ac.at
Phone: +43 1 58801 37601
Fax: +43 1 58801 37699

Copyright notice:

This is the authors' version of a work that was accepted for publication in *Proceedings of the 4th IFAC Workshop on Mining, Mineral and Metal Processing (MMM)*. Changes resulting from the publishing process, such as peer review, editing, corrections, structural formatting, and other quality control mechanisms may not be reflected in this document. Changes may have been made to this work since it was submitted for publication. A definitive version was subsequently published in F. Schausberger, K. Speicher, A. Steinboeck, M. Jochum, and A. Kugi, "Two illustrative examples to show the potential of thermography for process monitoring and control in hot rolling", in *Proceedings of the 4th IFAC Workshop on Mining, Mineral and Metal Processing (MMM)*, vol. 48, Oulu, Finland, 2015, pp. 48–53. DOI: 10.1016/j.ifacol.2015.10.076

ACIN

Two Illustrative Examples to Show the Potential of Thermography for Process Monitoring and Control in Hot Rolling

Florian Schausberger * **Katrin Speicher** *
Andreas Steinboeck * **Martin Jochum** ** **Andreas Kugi** *

* *Automation and Control Institute, Vienna University of Technology, Vienna, Austria (e-mail: {schausberger,speicher,steinboeck,kugi}@acin.tuwien.ac.at)*
** *AG der Dillinger Hüttenwerke, Dillingen, Germany (e-mail: martin.jochum@dillinger.biz)*

Abstract: This paper deals with the systematic analysis of thermographic images recorded during the hot rolling process of steel plates. In the first part, local disturbances are detected and different approaches for disturbance rejection are proposed. From the processed images, reliable mean temperature profiles in longitudinal and lateral direction are calculated. In the second part of the paper, an optimization problem is formulated and solved to calculate the plate velocity from the thermographic images. The approach proves to be a robust estimation method for the plate velocity. As the thermographic camera is already installed for temperature measurements, no additional measurement devices are needed so that investment and maintenance costs are saved.

Keywords: Thermography, hot rolling, temperature measurement, rolling speed, image processing, unconstrained optimization

1. INTRODUCTION

Thermographic cameras are widely used in very different fields ranging from medicine to building inspection, process monitoring, and non-destructive testing. Numerous application examples can be found in literature, which is reviewed for instance by Usamentiaga et al. (2014). There also a general introduction to infrared thermography is given.

Thermography has two major advantages in comparison with other temperature measurement methods: First, it is a non-contact and non-invasive technique, i.e., it can be used to measure the temperature of very hot or moving objects from a safe distance, which also simplifies maintenance. Second, the provided temperature measurements are two-dimensional and contain far more information than, e.g., single-point pyrometer or thermocouple measurements. These advantages render thermography also a promising measurement technique in the steel industry. There, it is used in laboratory experiments but also on-line during the production. For example, Vidoni et al. (2014) use thermocameras in their experimental strip caster in addition to pyrometers because they provide information about the temperature distribution across the width. The two-dimensional character of the measurement is also exploited by He et al. (2011), who employ thermography to experimentally characterize the scale formed on steel surfaces. In a work presented by Koch and Schroeder (2012), hot spots are detected in real-time thermographic images of hot-rolled steel billets for quality assessment. Their time evolution is analyzed to identify material flaws and to prevent false indications. Viale et al. (2007) also use infrared cameras for on-line detection of hot spots on ladles. Furthermore, the slag is automatically detected during tapping operation.

Summarizing, most of those applications use thermographic cameras for one single measurement purpose and thus exploit only a small part of the information contained in the two-dimensional images. However, different applications of thermography are simultaneously possible using the same image. This includes, e.g., the estimation of the velocity of moving objects or tracking of hot plates during their production. If images captured by several cameras, which cover the whole production line, are utilized, even more possibilities are opened up.

This paper aims at extending the scope of thermography in hot rolling. Since the large number of possible applications cannot be discussed in a single paper, this paper focuses on two different possible applications of thermographic imaging in hot rolling of heavy plates. Section 2 deals with the most obvious possibility, namely the temperature measurement. Using standard image processing techniques, local disturbances are removed from the image so that reliable mean lateral and longitudinal surface temperature profiles can be calculated. Furthermore, characteristic striped patterns can be extracted. Section 3 presents a fast and robust optimization-based estimation strategy for the plate velocity. The proposed method utilizes the non-uniformities of the plate surface temperature in the longitudinal direction. Note that both applications rate the same information, i.e., temperature inhomogeneities,

Post-print version of the article: F. Schausberger, K. Speicher, A. Steinboeck, M. Jochum, and A. Kugi, "Two illustrative examples to show the potential of thermography for process monitoring and control in hot rolling", in *Proceedings of the 4th IFAC Workshop on Mining, Mineral and Metal Processing (MMM)*, vol. 48, Oulu, Finland, 2015, pp. 48–53. DOI: 10.1016/j.ifacol.2015.10.076
The content of this post-print version is identical to the published paper but without the publisher's final layout or copy editing.

in a different way: While they are removed prior to the calculation of representative temperature profiles, they are vital for the estimation of the plate velocity.

2. CHARACTERIZATION OF THE PLATE SURFACE TEMPERATURE

In steel industry, the temperature evolution of the steel product during its production significantly influences its final quality. Therefore, it is crucial that the temperature is monitored and controlled. To this end, temperature sensors are installed at many different positions in the production process, cf. Peacock (1999). In hot rolling, pyrometers are used in most cases, see, e.g., Zheng and Li (2011), Speicher et al. (2014), and the references given therein. However, pyrometers normally measure only on the centerline of the product and do not provide information about the lateral temperature profile, which, for instance, is an important quantity for the adjustment of the water distribution in the cooling section. This drawback can be overcome by using thermographic cameras instead of pyrometers. From the two-dimensional temperature measurements, a mean lateral temperature profile can be calculated. Additionally, the mean longitudinal temperature profile is more reliable than the pyrometer recordings, which are obtained while the product moves through the measuring ray of a pyrometer, because it is less affected by local disturbances, e.g., scale spots.

2.1 Identification of local disturbances

Before averaging the rows and columns of the thermographic image, local disturbances, which may arise from production inhomogeneities, reflection, or obstacles in the field of view of the camera, should be eliminated first. Since all production steps affect the plate temperature either in lateral or in longitudinal direction, it can be assumed that the disturbances are the only part in the measured temperature distribution, which depends on both coordinates. Hence, the measured surface temperature $T\left(x,z\right)$ is assumed to be composed of four parts, i.e.,

$$T\left(x,z\right)=T_m+T_x(x)+T_z(z)+T_d\left(x,z\right). \tag{1}$$

Thus, the local disturbances $T_d\left(x,z\right)$ are separated from the mean temperature T_m, and the longitudinal and lateral striped pattern T_z and T_x, which depend only on the lateral coordinate z or the longitudinal coordinate x, respectively. Images with raster size $M\times N$ contain only temperature values at $x_j=j\delta, j=1,\dots,M$, and $z_i=i\delta, i=1,\dots,N$ with the pixel size δ. The spatially discretized temperature field $T(x_j,z_i)$ can be expressed by the inverse two-dimensional cosine transform (cf. Jain (1989))

$$\begin{aligned}T(x_j,z_i)=&\sum_{n=1}^{N}\sum_{m=1}^{M}C_{nm}\alpha_n\cos\left(\frac{\pi\left(2i-1\right)\left(n-1\right)}{2N}\right)\\&\cdot\beta_m\cos\left(\frac{\pi\left(2j-1\right)\left(m-1\right)}{2M}\right),\end{aligned} \tag{2}$$

which is a standard tool in image processing and compression. The amplitude of the individual cosine functions depends on the coefficients C_{nm} and the parameters

$$\begin{aligned}\alpha_1&=\frac{1}{\sqrt{N}},\quad \alpha_n=\frac{2}{\sqrt{N}},\quad n=2,\dots,N\\ \beta_1&=\frac{1}{\sqrt{M}},\quad \beta_m=\frac{2}{\sqrt{M}},\quad m=2,\dots,M.\end{aligned} \tag{3}$$

Hence, the size of the image determines the frequency resolution of (2) as well as the values (3).

The double sum in (2) is rearranged in the form

$$\begin{aligned}T(x_j,z_i)=&C_{11}\alpha_1\beta_1\\&+\sum_{n=2}^{N}C_{n1}\alpha_n\beta_1\cos\left(\frac{\pi\left(2i-1\right)\left(n-1\right)}{2N}\right)\\&+\sum_{m=2}^{M}C_{1m}\alpha_1\beta_m\cos\left(\frac{\pi\left(2j-1\right)\left(m-1\right)}{2M}\right)\\&+\sum_{n=2}^{N}\sum_{m=2}^{M}C_{nm}\alpha_n\cos\left(\frac{\pi\left(2i-1\right)\left(n-1\right)}{2N}\right)\\&\cdot\beta_m\cos\left(\frac{\pi\left(2j-1\right)\left(m-1\right)}{2M}\right).\end{aligned} \tag{4}$$

By comparison with (1), it can be seen that the information about the local disturbances is contained in the coefficients $C_{nm}, n=2,\dots,N, m=2,\dots,M$. Using this assumption, reliable mean temperature profiles are calculated in the next section. Furthermore, striped lateral and longitudinal patterns can be calculated by evaluating only the second or the third term in (4).

2.2 Calculation of a mean lateral temperature profile

In the following, the thermographic image shown in Fig. 1 is considered to demonstrate the proposed algorithms. In this figure as well as in the following ones, the plate temperature is normalized to the maximum temperature $T_{\max}$. Since the cosine transform (4) requires a rectangular

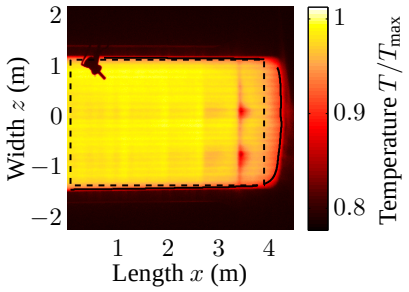

Fig. 1. Original thermographic image with detected edges (solid black line) and selected section for image processing (dashed black line).

section of the plate, the edges of the plate are first detected by an extension of the Canny algorithm (cf. Canny (1986)) and the largest rectangular section inside the identified edges is then selected for the presented analyses. The selected section is shown in Fig. 2(a) and contains two disturbances: two colder spots at the head end of the plate and a pyrometer in the upper left corner. The cold spots may result from water pools on the non-flat surface. In contrast to the cold spots, the pyrometer is a systematic disturbance and is always inside the field of view of the camera. Both disturbances can be extracted

Post-print version of the article: F. Schausberger, K. Speicher, A. Steinboeck, M. Jochum, and A. Kugi, "Two illustrative examples to show the potential of thermography for process monitoring and control in hot rolling", in *Proceedings of the 4th IFAC Workshop on Mining, Mineral and Metal Processing (MMM)*, vol. 48, Oulu, Finland, 2015, pp. 48–53. DOI: 10.1016/j.ifacol.2015.10.076
The content of this post-print version is identical to the published paper but without the publisher's final layout or copy editing.

by calculating only the last term of (4). However, the resulting image of disturbances also contains artifacts due to the limited frequency resolution, cf. the yellow stripes in Fig. 2(b). Therefore, subtracting Fig. 2(b) from Fig. 2(a) removes the two major disturbances in the selected section, but it also causes some artificial non-uniformities, see Fig. 2(c). To avoid some of these artificial disturbances, a threshold $T_{d,\min}$ may be imposed on the disturbance image (Fig. 2(b)) so that only disturbances larger than the threshold are subtracted from the original section in Fig. 2(a). However, the definition of a general threshold is challenging because the disturbances vary from image to image. Finally, the processed image Fig. 2(c) is reinserted in the dashed section in Fig. 1 before the mean lateral temperature profile is calculated.

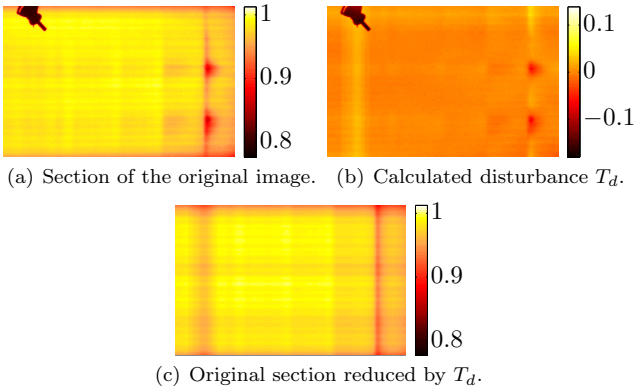

(a) Section of the original image. (b) Calculated disturbance T_d.

(c) Original section reduced by T_d.

Fig. 2. Image processing of the selected section.

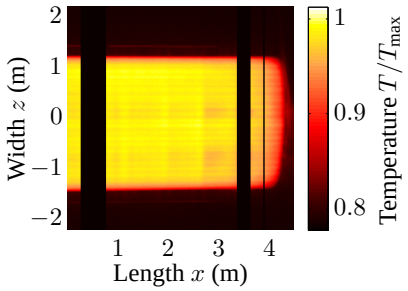

Fig. 3. Original thermographic image with deleted columns.

Since this kind of disturbance rejection, which is referred to as *first approach* in the following, may be unsatisfactory, a *second approach* is adopted. In the disturbance image of Fig. 2(b), columns with large standard deviation are identified; then, the corresponding columns in Fig. 1 are deleted, see Fig. 3, and not considered in the calculation of the mean lateral temperature profile.

Fig. 4 compares the mean lateral temperature profiles obtained by the two approaches with the one calculated from Fig. 1 without any disturbance rejection. For clarity reasons, the differences resulting from both disturbance rejection approaches are also shown in Fig. 5. While deleting the columns with large disturbances leads to large changes, subtracting the disturbance image leaves the mean temperature profile nearly unchanged. Furthermore, the first approach artificially homogenizes the image in longitudinal

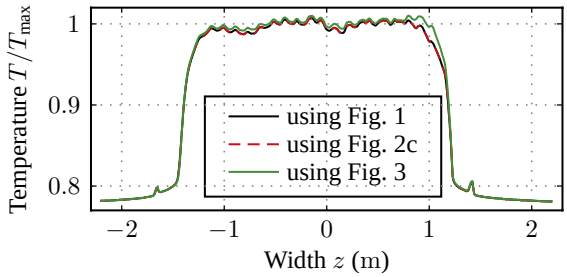

Fig. 4. Mean lateral temperature profiles calculated from the original image (Fig. 1, black), the original image reduced by the disturbance (Fig. 2(c), red), and the original image with deleted columns (Fig. 3, green).

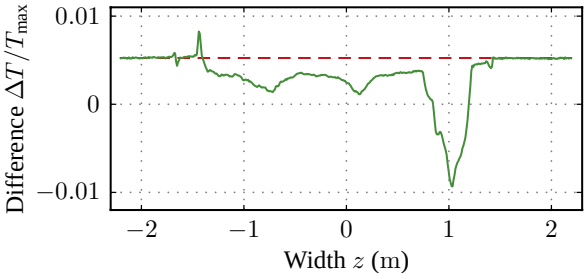

Fig. 5. Differences between the mean lateral temperature profile calculated from the original image and the ones calculated from the processed images of Fig. 2(c) (red) and Fig. 3 (green).

direction so that the standard deviation barely depends on the lateral coordinate z, see Fig. 6. Note that the regions close to the edges remain unaffected by the first approach because they are not contained in Fig. 2(c), i.e. the corresponding section with the dashed boundary in Fig. 1. It can be concluded that the first approach may lead to a

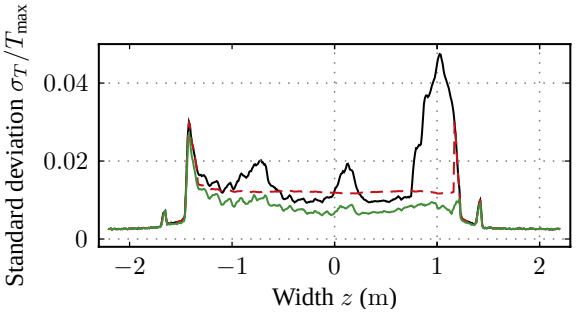

Fig. 6. Standard deviation of the mean lateral temperature profiles of Fig. 4.

better image without disturbances at first sight but it does not improve the reliability of the calculated lateral profile. By contrast, the standard deviation is significantly reduced by the second approach although only a few columns were deleted from the original image. Consequently, deleting some parts of the image, which are selected based on the disturbance image, leads to a more reliable mean lateral temperature profile.

Of course, the proposed approach can be also be used to calculate a mean longitudinal temperature profile. Then, rows are deleted from the original image prior to averaging.

Post-print version of the article: F. Schausberger, K. Speicher, A. Steinboeck, M. Jochum, and A. Kugi, "Two illustrative examples to show the potential of thermography for process monitoring and control in hot rolling", in *Proceedings of the 4th IFAC Workshop on Mining, Mineral and Metal Processing (MMM)*, vol. 48, Oulu, Finland, 2015, pp. 48–53. DOI: 10.1016/j.ifacol.2015.10.076
The content of this post-print version is identical to the published paper but without the publisher's final layout or copy editing.

3. ESTIMATION OF THE PLATE VELOCITY

During rolling, the thickness of steel slabs is reduced in consecutive roll passes to a desired final plate thickness. In this process, the entry and exit speed of the plate are important quantities. They may be used, e.g., to calculate the relative change of the plate thickness during the roll pass based on the mass balance. Furthermore, the exit speed of the plate may be used to calculate the already rolled part of the plate in the current pass. Its precise knowledge is required when applying disturbance feedforward control strategies as proposed in Heeg et al. (2007). Consequently, the plate velocity has to be measured or estimated.

3.1 Existing velocity estimation methods

Measurement methods for the velocity may be divided into indirect and direct measurement principles, see, e.g., Ginzburg and Ballas (2000):

- Indirect methods determine the velocity of the plate by using measurements of the angular velocity of the work rolls.
- Direct methods aim at directly measuring the velocity of the plate.

Indirect methods are prone to errors due to the generally inexact knowledge of the slip between the plate and the rolls. However, this slip can be accurately calculated by using tailored mathematical models, see, e.g., Kiefer and Kugi (2008).

Direct measurement methods typically achieve a higher accuracy. However, additional sensors are needed. A common measurement principle is based on a laser sensor utilizing the Doppler effect. The laser beam is optically split into two beams which are projected on the same point of the plate. This measurement setup yields a non-perpendicular alignment between the beams and the surface of the plate in the rolling direction. Due to the moving plate, the frequency of the scattered beams is shifted by a small amount depending on the velocity of the plate. The velocity is determined by measuring this so called Doppler frequency (cf. Isei et al. (2006); Engman et al. (2012)).

A velocity sensor should be located as near as possible to the roll gap because the velocity of short plates should also be measured. However, such an assembly is affected by steam, dust, and heat and requires costly robust sensors.

As already discussed before, thermographic cameras are often used to measure the surface temperature of rolled products. This measurement device may also be exploited to determine the velocity of the plate. In this work, the thermographic camera mounted above the plate behind the finishing mill of the heavy plate mill at the AG der Dillinger Hüttenwerke will be utilized for this purpose. The infrared CCD camera captures images (cf. Fig. 1) of the plate with a fixed sampling time $T_s = 1/30$ s and an image resolution of $M \times N = 659 \times 494$ pixels. The use of a two-dimensional temperature distribution instead of a spot-like laser scanner is beneficial in terms of robustness against disturbances, e.g., caused by steam.

3.2 Optimization-based detection of the plate velocity

As shown in Fig. 1, the surface temperature distribution $T(x, z)$ is generally non-uniform in the longitudinal direction x of the plate. These inhomogeneities may be caused by non-uniform heating in the slab furnace or inhomogenous conditions during the rolling process. Contrary to Section 2, these imperfections are advantageous and even necessary to determine the velocity of the plate by the proposed method.

To this end, the mean surface temperature in lateral direction

$$\bar{T}(x_j, t_k) = \frac{1}{L+1} \sum_{i=i_0-L/2}^{i_0+L/2} T(x_j, z_i)\Big|_{t=t_k} \tag{5}$$

of the image captured at time $t = t_k$ is calculated. The averaging in (5) utilizes a rectangular section of the image with $L + 1$ rows symmetric to the row i_0. Note that spatially fixed systematic disturbances, e.g., the pyrometer, must not be contained in this section of the image. Instead of the mean temperature distribution, it would also be possible to use the temperature values from a single row of the image. However, the larger number of measurements improves the robustness of the estimation against noise and local disturbances.

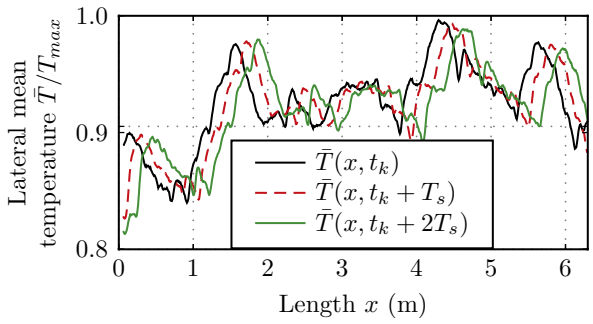

Fig. 7. Mean temperature distribution for three consecutive images.

As an example, the resulting longitudinal temperature distribution for three consecutive images with $L = 20$ is shown in Fig. 7. Since the images are captured with a high frame rate, the temperature of the plate of consecutive images is almost the same. The figure suggests that there is only a spatial shift of a more or less constant temperature distribution. In this case, the shift Δx between the distributions can be determined, e.g., by using the cross correlation function (see, e.g., Orfanidis (1996)). Assuming a constant velocity within a sampling time T_s, the velocity of the plate v_{PL} results in

$$v_{PL} = \frac{\Delta x}{T_s}. \tag{6}$$

However, the temperature distribution is subject to disturbances. Possible reasons are heat conduction processes or image distortions caused by the optical lens of the camera. Such disturbances entail additional deviations between the shifted temperature profiles and therefore deteriorate the velocity estimation, unless they are systematically considered in the estimation approach. From experience it is

Post-print version of the article: F. Schausberger, K. Speicher, A. Steinboeck, M. Jochum, and A. Kugi, "Two illustrative examples to show the potential of thermography for process monitoring and control in hot rolling", in *Proceedings of the 4th IFAC Workshop on Mining, Mineral and Metal Processing (MMM)*, vol. 48, Oulu, Finland, 2015, pp. 48–53. DOI: 10.1016/j.ifacol.2015.10.076
The content of this post-print version is identical to the published paper but without the publisher's final layout or copy editing.

known that these distortions depend on the spatial coordinate x of the image. Therefore, the empirical approach

$$\hat{T}(x,t_k) = p(x)\bar{T}(x,t_k), \tag{7}$$

with a scaling function (polynomial)

$$p(x) = \sum_{n=0}^{N_p} a_n x^n \tag{8}$$

with degree N_p and so far unknown coefficients a_n, is employed to compute an undistorted temperature distribution $\hat{T}(x,t_k)$. As the temperature distribution (5) is only defined at the grid points x_j, $j = 1,\dots,M$, a linear interpolation is performed in (7) between the pixels to achieve sub-pixel resolution.

A convenient method of determining the velocity of the plate and the unknown polynomial coefficients a_n in (8) is to minimize the difference $e(x,t_k;\Delta x,\mathbf{p})$ between consecutive temperature distributions. At time t_k, this error is defined as

$$e(x,t_k;\Delta x,\mathbf{p}) = \hat{T}(x-\Delta x, t_k - T_s) - \hat{T}(x,t_k) \tag{9}$$

$\forall x \in [\Delta x, l_{FOV} - \Delta x]$ with the coefficient vector $\mathbf{p} = \begin{bmatrix} a_1 & a_2 & \cdots & a_{N_p} \end{bmatrix}^{\mathrm{T}}$ and the length of the camera's field of view l_{FOV}.

The first coefficient is chosen as $a_0 = 1$ because it would only scale the temperature distribution $\bar{T}$ by a constant factor. Hence, a static optimization problem can be formulated as

$$\min_{\Delta x,\, \mathbf{p} \in \mathbb{R}^{N_p}} \quad \sum_{k=1}^{K-1} \sum_{j=1}^{M} e^2(x_j,t_k;\Delta x,\mathbf{p}) \tag{10}$$

using M nodes of K images. Note that only the spatially overlapping parts of the temperature difference in (9) are used in (10). Clearly, an implicit assumption made here is that the velocity is constant during the time interval $t_0 \le t \le t_{K-1}$. Therefore, the time interval should not be too large. On the other hand, increasing the number K of consecutive images reduces noise in the estimation result, which is why a compromise has to be found. Once the optimization problem (10) is solved, the velocity of the plate follows from (6).

3.3 Numerical solution of the optimization problem

The Gauß-Newton method, see, e.g., Nocedal and Wright (2006), is used for solving the optimization problem (10). This method was chosen because of its superlinear convergence rate and the fact that it only requires the evaluation of the Jacobian $\mathbf{J}$ in every iteration. Let the Jacobian $\mathbf{J}$ of $\mathbf{e}$ with respect to $\mathbf{w}$ be denoted as $\mathbf{J}(\mathbf{w}) = (\nabla \mathbf{e})^{\mathrm{T}}$ with the vector of optimization variables $\mathbf{w} = \begin{bmatrix} \Delta x & \mathbf{p}^{\mathrm{T}} \end{bmatrix}^{\mathrm{T}}$ and

$$\mathbf{e} = \left[e(x_1,t_1;\Delta x,\mathbf{p}) \;\; \dots \;\; e(x_M,t_{K-1};\Delta x,\mathbf{p}) \right]^{\mathrm{T}}.$$

The Gauß-Newton method is based on the iterative update law

$$\mathbf{w} \leftarrow \mathbf{w} - \underbrace{\left(\mathbf{J}^{\mathrm{T}}(\mathbf{w})\mathbf{J}(\mathbf{w})\right)^{-1}\mathbf{J}^{\mathrm{T}}(\mathbf{w})\mathbf{e}}_{\boldsymbol{\Delta}\mathbf{w}}.$$

The method terminates if the maximum number of iterations is exceeded or the convergence criterion $\|\boldsymbol{\Delta}\mathbf{w}\|_\infty < \gamma$ with a properly chosen constant $\gamma > 0$ is fulfilled.

The derivative of $e(x_j,t_k;\Delta x,\mathbf{p})$, $j = 1,\dots,M$ and $k = 1,\dots,K-1$ with respect to $\mathbf{w}$ is required in $\nabla\mathbf{e}$ and can be calculated using a Savitzky-Golay filter, see, e.g., Orfanidis (1996), with degree 2 and window length 11.

3.4 Measurement results

In the following, results from a plate rolled in the heavy plate mill of the AG der Dillinger Hüttenwerke are presented. As an initial guess $\mathbf{w}_0$ for the optimization, the result from the previous run is used. In the first optimization, $\Delta x_0 = v_{PL,0} T_s$ with $v_{PL,0} = 2$ m/s and $\mathbf{p}_0 = \mathbf{0}$ are chosen as initial values. The parameters used for the computations are listed in Tab. 1.

Table 1. Parameters of the velocity estimation.

Parameter	Value	Unit
L	20	
i_0	494/2	
M	659	
K	5	
T_s	1/30	s
γ	10^{-3}	
l_{FOV}	6.3475	m

In Fig. 8, the estimated plate velocity is shown with ($N_p = 5$) and without ($N_p = 0$) compensation of the disturbances. Furthermore, the number of iterations needed until the convergence criterion was satisfied is depicted in the lower picture. It is known that the angular velocity of the work rolls was kept constant during the roll pass, which is in accordance with the results using the compensation. Without compensation of the disturbances, an inaccurate estimation result is obtained. At the end of the roll pass ($t \ge 10$ s), the plate is decelerated.

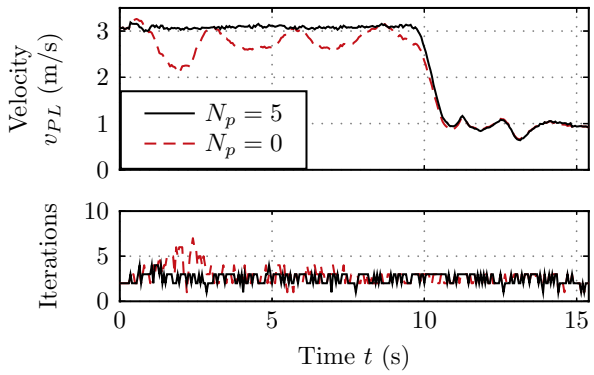

Fig. 8. Estimated speed and performed optimization iterations for a rolled plate with and without disturbance compensation.

Since there is no other velocity measurement device installed at the considered rolling mill, the estimated velocity is validated by means of the plate length. The estimated plate length l_{est} follows in the form

$$l_{est} = \int_{t_1}^{t_2} v_{PL}\mathrm{d}t + l_{FOV} = 42.8918 \text{ m}$$

with the integration boundaries $t_1 = 0$ and $t_2 = 15.4$ s. The time t_1 defines the exit of the head end and t_2 the

Post-print version of the article: F. Schausberger, K. Speicher, A. Steinboeck, M. Jochum, and A. Kugi, "Two illustrative examples to show the potential of thermography for process monitoring and control in hot rolling", in *Proceedings of the 4th IFAC Workshop on Mining, Mineral and Metal Processing (MMM)*, vol. 48, Oulu, Finland, 2015, pp. 48–53. DOI: 10.1016/j.ifacol.2015.10.076
The content of this post-print version is identical to the published paper but without the publisher's final layout or copy editing.

entry of the tail end of the plate in the camera's field of view, respectively.

Measurement data from a downstream contour measurement device is used to determine the actual plate length $l = 42.4551$ m. The good agreement of l and l_{est} (relative error $\approx 1\%$) indicates that the average velocity was accurately estimated. Although only the rolling speed of one representative plate is shown in this paper, similar results have been observed for other randomly chosen plates. With the presented parameters, it takes less than 3 ms (Standard PC with i7-2600 @ 3.4 GHz processor and 16 GB RAM) to solve the optimization problem (10) in MATLAB at a time t_k.

4. CONCLUSIONS

In this paper, thermographic images of hot plates were analyzed to extract important information for process control. All images were recorded during standard production by an industrial thermographic camera mounted above the production line.

In the first part, the cosine transform was applied to extract systematic as well as non-systematic local disturbances from the image. After disturbance rejection, mean temperature profiles in lateral direction were calculated. These average profiles are more reliable compared to the usual single point pyrometer measurements.

In the second part, an optimization-based approach to estimate the plate velocity is presented. To this end, inhomogeneities of the measured plate temperature in longitudinal direction are utilized. As the measured temperature is subject to disturbances, an empirical correction using a polynomial scaling function is performed. The optimization problem is solved by means of the Gauß-Newton method within a few iterations.

The discussed temperature measurements and velocity estimations are not the only possible applications of the thermographic images: They may also be advantageously used for control and process monitoring tasks. If, for example, a deviation between the desired and the actual plate contour is detected in an image, the contour information can be fed back to the mill stand to adjust the roll gap of the next pass so that the deviation is eliminated, see, e.g., Schausberger et al. (2015). In view of process monitoring and maintenance, the cosine transform also proves to be useful. Recurrent longitudinal stripes can be detected and ascribed to deficient descaling caused by failure of descaling nozzles. Finally, it should be emphasized that the use of an existing measurement device for several measurement tasks saves investment and maintenance costs.

ACKNOWLEDGEMENTS

The third author gratefully acknowledges financial support provided by the Austrian Academy of Sciences in the form of an APART-fellowship at the Automation and Control Institute of Vienna University of Technology.

REFERENCES

Canny, J. (1986). A computational approach to edge detection. *IEEE Transactions on Pattern Analysis and Machine Intelligence*, 8, 679–698.

Engman, M., Falkenström, M., and Kimab, S. (2012). Novel technique for velocity and thickness measurements with laser ultrasonics. In *18th World Conference on Nondestructive Testing*. Durban, South Africa.

Ginzburg, V. and Ballas, R. (2000). *Flat Rolling Fundamentals*. Marcel Dekker.

He, Y., Tian, G., Cheng, L., Zhang, H., and Jackson, P. (2011). Parameters influence in steel corrosion evaluation using PEC thermography. In *Proc. of the 17th Int. Conf. on Automation and Computing*, 255–260. Huddersfield, UK.

Heeg, R., Kiefer, T., Kugi, A., Fichet, O., and Irastorza, L. (2007). Feedforward control of plate thickness in reversing plate mills. *IEEE Transactions on Industry Applications*, 43(2), 386–394.

Isei, Y., Yakita, Y., and Buei, Y. (2006). Development of interstand velocimeter for hot strip finishing mill. In *SICE-ICASE 2006, Int. Joint Conference*, 2508–2511. Busan, South Korea.

Jain, A.K. (1989). *Fundamentals of Digital Image Processing*. Prentice-Hall.

Kiefer, T. and Kugi, A. (2008). An analytical approach for modelling asymmetrical hot rolling of heavy plates. *Mathematical and Computer Modelling of Dynamical Systems*, 14(3), 249–267.

Koch, S. and Schroeder, J. (2012). In-line inspection of hot-rolled steel billets by heat flux thermography. In *Proc. of the 18th World Conference on Nondestructive Testing*. Durban, South Africa.

Nocedal, J. and Wright, S.J. (2006). *Numerical Optimization*. Springer Series in Operations Research. Springer.

Orfanidis, S. (1996). *Optimum Signal Processing: An Introduction*. Prentice Hall, New York.

Peacock, G.R. (1999). Review of noncontact process temperature measurement in steel manufacturing. In *Proc. of SPIE, Thermosense XXI*, volume 3700, 171–189. Orlando, USA.

Schausberger, F., Steinboeck, A., and Kugi, A. (2015). Mathematical modeling of the contour evolution of heavy plates in hot rolling. *Applied Mathematical Modelling*. (in press).

Speicher, K., Steinboeck, A., Wild, D., Kiefer, T., and Kugi, A. (2014). An integrated thermal model of hot rolling. *Mathematical and Computer Modelling of Dynamical Systems*, 20(1), 66–86.

Usamentiaga, R., Venegas, P., Guerediaga, J., Vega, L., Molleda, J., and Bulnes, F.G. (2014). Infrared thermography for temperature measurement and nondestructive testing. *Sensors*, 14(7), 12305–12348.

Viale, M., Martin, O., Muratori, F., Bertezzolo, U., Perez, J., and Usart, J. (2007). Application of on-line infrared thermography in steel making industry. In *Proc. of SPIE, Thermosense XXIX*, volume 6541. Orlando, USA.

Vidoni, M., Mendel, A., and Hirt, G. (2014). Profile strip casting with inline hot rolling: Numerical simulations for the process chain design. *Key Engineering Materials*, 1568–1575.

Zheng, Y. and Li, S. (2011). Plant-wide temperature drop monitoring in run-out table strip cooling process. In *Proc. of the Int. Symposium on Advanced Control of Industrial Processes ADCONIP*, 287–292. Hangzhou, China.

Post-print version of the article: F. Schausberger, K. Speicher, A. Steinboeck, M. Jochum, and A. Kugi, "Two illustrative examples to show the potential of thermography for process monitoring and control in hot rolling", in *Proceedings of the 4th IFAC Workshop on Mining, Mineral and Metal Processing (MMM)*, vol. 48, Oulu, Finland, 2015, pp. 48–53. DOI: 10.1016/j.ifacol.2015.10.076
The content of this post-print version is identical to the published paper but without the publisher's final layout or copy editing.